Monte Carlo Simulations of Probe−Host Chain Entanglement: Influence of Host Mobility and Size on Probe Electrophoretic Motion

M. E. Starkweather, M. Muthukumar,* and D. A. Hoagland

Department of Polymer Science and Engineering and Materials Research Science and Engineering Center (MRSEC), University of Massachusetts, Amherst, Massachusetts 01003

Received April 1, 1999; Revised Manuscript Received July 12, 1999

ABSTRACT: A Monte Carlo method simulates chain trajectories during the pairwise configurational interactions of a single field-driven polyelectrolyte "probe" chain and a single neutral "host" chain. The goal is to understand how the mobility and chain length of dilute, neutral polymers affect the separation of dilute polyelectrolytes during capillary electrophoresis in a neutral polymer solution. The simulations fix probe charge density, Debye−Hückel screening length, and probe−host starting displacement, but vary chain length from 50 to 200 and 70 to 200 Kuhn steps, respectively, for flexible probe and hosts. Many trajectories lead to probe−host chain entanglement, an event believed responsible for the polyelectrolyte size discrimination observed in actual experiments. Chain distortions in response to such entanglement frequently produce double hairpin configurations that persist until the shortest hairpin arm slides past the locus of entanglement. Average probe velocity exhibits a minimum when probe and host chain lengths are nearly equal. The minimum reflects an interplay of two effects: the average duration of entanglement, which by increasing with probe length reduces mobility, and the average displacement of an entanglement, which by increasing with probe length raises mobility.

1. Introduction

Capillary electrophoresis of both biological and synthetic polyelectrolytes in dilute neutral polymer solutions can provide fast and efficient analytical separations by chain length.[1−5] In many cases, the separations compare favorably with those obtained in gels and concentrated neutral polymer solutions. The success of the dilute neutral polymer approach is remarkable in at least two respects. First, unlike other media used to fractionate polymer solutes by chain length, these solutions display the fluidity of a low molecular weight solvent. Second, a solution populated by a nonoverlapping concentration of neutral polymers does not possess a feature essential to conventional theories for electrophoretic separation, a pore matrix. The configurational interactions responsible for polyelectrolyte separation in this nonconfining environment are not yet well understood. We believe that new physical insights can be gained by simulating the field-biased chain trajectories of a simple model, one consisting of a single flexible polyelectrolyte "probe" and a single flexible neutral polymer "host".

Although the use of dilute or semidilute neutral polymer solutions for separating polyelectrolytes is relatively new, the potential importance of the scheme has already motivated several parameter studies. The influence of host chain stiffness,[6,7] host polydispersity,[7−9] host concentration,[2,4,10] host and probe molecular weight,[1,6,11] medium ionic strength,[12] and probe−host complexation[13] have been evaluated to varying extent by experiment. While each significantly modifies probe mobility, a theory integrating and explaining the combined influence all parameters has not been constructed. The most successful molecular-level description for these separations is a scaling-type analysis developed by Hubert et al.[14] for a single mode of probe−host configurational interaction. Of the experimental observations reported in the literature, the most pertinent to the current study is the finding that higher molecular weight neutral polymers better separate higher molecular weight probe polymers.[4,11,15] Via our simulations, we hope to explain this trend in terms of the molecular weight−dependent configurational interactions of probe and host polymers.

We study by Monte Carlo simulation the configurational interactions of a flexible polyelectrolyte probe chain as it migrates in a uniform electrical field around and through a flexible neutral host chain. Both probe and host are constructed as three-dimensional, off lattice random walks. The applied field is of intermediate strength and able to deform the chains only when they are entangled. Even in this state, however, configurational fluctuations play an important role in the eventual release of entanglement. Our approach neglects the complex hydrodynamics of the chain pair but captures the essence of their more important configurational interactions. Initial placement of probe and host with closely spaced centers of mass aligned along the field direction causes the probe to collide and then drag the host downfield in a high fraction of the simulated trajectories. Electrostatic interactions are modeled through Debye−Hückel screening, and all overlapping chain configurations are disallowed. The current simulations improve upon those previously reported by us,[16] as the host chains are now given both flexibility and mobility; in the earlier report these chains were frozen. With the improvement, both probe and host are treated in a configurationally consistent manner, a major step toward our ultimate goal, a quantitative comparison of theory/simulation results to actual experiments.

The Monte Carlo simulations presented here complement the Brownian dynamics simulation[17,18] of collisions of a field-driven polymer with a finite-sized obstacle. Although the underlying mechanisms of "unhooking" and "rolling off" can be visualized easily in an isolated post or obstacle, we study the collective effect introduced by the connectivity of the host polymer. In the present three-dimensional simulations, we moniter the interplay

10.1021/ma990478r CCC: $18.00
Published on Web 09/18/1999

between the configurations of both the probe and the host.

2. Model and Simulation

The Monte Carlo simulation algorithm represents the mobile probe and host as pearl-necklace chains of lengths N and M, respectively, with repect to Kuhn step length l. This length is the same for both the probe and the host. The chains are freely jointed, freely rotating, and three-dimensional. Each bead possesses a hard core diameter α large enough to prevent bond crossings during equilibration and simulated electrophoresis dynamics. Thus, monomers i and j, separated by distance $r_{i,j}$ experience a binary hard core repulsion V_1:

$$V_1(r_{ij}) = \begin{cases} 0 & \text{if} \quad r_{ij} > \alpha \\ \infty & \text{if} \quad r_{ij} \leq \alpha \end{cases} \tag{1}$$

Note that the indices i and j extend over both chains. All beads on the probe chain are endowed with a unit charge, and the beads repel each other through a dimensionless Debye−Hückel potential,

$$V_2(r_{ij}) = \beta \frac{q_i q_j}{r_{ij}} \exp(-\kappa r_{ij}) \tag{2}$$

where $q = +1$, and κ^{-1} is the electrostatic screening or Debye length, a parameter equated to l in the simulations but dictated in actual experiments by the concentration of dissolved ions,

$$\kappa^2 = 4\pi\beta \sum_i c_i z_i^2 \tag{3}$$

where c_i and z_i are the concentration and valence, respectively, of the ith ion. Two unscreened unit charges separated by a Bjerrum length β interact with the ambient thermal energy, i.e.,

$$\beta = \frac{e^2}{4\pi\epsilon_0\epsilon kT} \tag{4}$$

where e is the electron charge, ϵ is the solvent dielectric constant, ϵ_0 is the permittivity of vacuum, k is the Boltzmann constant, and T is the temperature. The value of β chosen for the simulations (7.14 Å) corresponds to water at 300 K ($\epsilon = 78$).

Probe and host chains move according to the kink-jump algorithm, with each configurational change initiated by motion of a backbone bead m selected randomly from either of the chains. If not at a chain end, the bead is rotated through a random angle ϕ about an axis defined by the bead's two nearest neighbors. If an end bead is selected, rotation of the terminal bond about two randomly chosen angles ϕ and θ determines the end bead's new position. All bead movements for probe and host satisfy inter- and intrachain excluded volume constraints. Simulated configurations that do not violate these constaints are sampled according to the Metropolis algorithm.[19] This algorithm accepts or rejects configurations based on the energy difference ΔE_m that accompanies a proposed configurational change,

$$\Delta E_m = \sum_{i<j}\sum_j V_2(r_{ij})_{\text{new}} - \sum_{i<j}\sum_j V_2(r_{ij})_{\text{old}} + qeE(X_{m,\text{new}} - X_{m,\text{old}}) \tag{5}$$

where the factor $X_{m,\text{new}} - X_{m,\text{old}}$ reflects bead displacement along a coordinate aligned with the electric field E. If $\Delta E_m < 0$, the proposed move is accepted automatically; otherwise, acceptance follows the statistical criterion

$$\exp\left(-\frac{\Delta E_m}{kT}\right) \geq w \tag{6}$$

where w is a random number from the interval (0,1). Whether accepted or rejected, each attempted move is counted, and N counts define a Monte Carlo (MC) time step. Simulations are carried out for $M = 70$, 100, and 200 and for $N = 50$, 60,70, 100, and 140. In the present simulations, the dimensionless field strength $qEl/k_BT = 0.1$ to avoid[16] any artificial effects that might arise from nonergodicity.

Before simulation of a chain pair configurational trajectory, probe and host are equilibrated, respectively, for greater than N^2 or M^2 MC time steps. Then, the two chains are placed in an initial run configuration with their two centers of mass aligned with the field direction and these centers displaced from each other by $10l$. During the subsequent simulation, the relative chain alignment and displacement obviously change. For example, random motion of either or both chains orthogonal to the field direction may produce a chain pair trajectory with no interesting features, i.e., with no interchain interactions. The constraints on the initial run configurations are necessary to suppress these uninteresting trajectories while avoiding starting configurations that superimpose probe and host. In a broader sense, the constraints applied to the starting configuration reflect a tradeoff between finite computer time and a desire to sample trajectories generated from the fullest set of starting configurations. We believe the current choice of initial run configurations achieves an optimal balance. Results are not reported here for the probability of entanglement for this set of starting configurations; these probabilities differ little from those described previously for a frozen host.[16] Across the range of N and M explored, between 20 and 90% of the simulations result in entanglement, with this percentage enhanced at larger values of N and M.

Only when the tailing bead of the probe exceeds the maximum downfield bead position of the host is a simulation terminated. For each run, data are gathered for both the duration of entanglement and the probe center of mass displacement during entanglement; runs without entanglement are discarded. As noted in a previous article,[16] the presence of an entanglement can be clearly discerned, either by visualization of the two chain configurations or by tracking the probe's center of mass movement versus time. To achieve adequate statistics, between 500 and 1000 independent simulations are executed for each probe and host chain length combination. For a sampling of runs, full bead position data have been stored at each time step, a memory-intensive procedure that enables a graphical presentation of the evolving pair trajectory.

3. Results

Figure 1 displays a typical configurational Monte Carlo trajectory for a probe−host entanglement interaction. Similar to the frozen host case described previously,[16] the probe eventually forms a well-defined locus where it loops around the host, forming a U-shaped

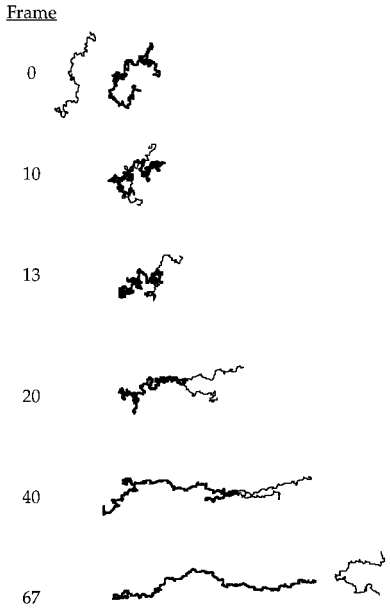

Figure 1. Representative chain pair trajectory for $N = 200$ and $M = 200$. The probe chain (drawn for clarity with the thinner backbone) migrates from left to right in a horizontally oriented electric field. The frame number provides the relative time position of the configurational state displayed.

hairpin with the two chain ends directed downfield. The force exerted on the probe is transferred effectively to the host at this locus, and the two chains are consequently dragged downfield together for the duration of the entanglement. New to the current simulation is the observation of a corresponding U-shaped hairpin conformation in the host. Together, these chain conformations create an oriented double hairpin configuration centered at the locus of contact. The two hooked chains slowly disengage by a pully-like process involving both chains. Random back-and-forth sliding of the two chains eventually leads to the release of one chain end. At the time of release, one chain typically extends linearly (without hairpin) in the field direction while the other chain retains its U shape; both distorted chain conformations only slowly relax as the chains move apart after release of entanglement. If two loci of contact begin to develop as the chains entangle, one of these loci rapidly disappears, leading to a chain trajectory similar to the one illustrated in Figure 1; these rare events are statistically irrelevant.

To monitor probe and host center of mass motion, the positions of these centers are recorded at intervals of 10 MC time steps. At the onset and disengagement of entanglement, the MC time step and the probe's center of mass position are recorded. In MC time steps, Figure 2 plots the average duration of an entanglement against N for $M = 70$, 100, and 140. This parameter remains strongly N-dependent only for $N < M$. The trend manifests the tendency for disentanglement by release of the shortest of the four hairpin arms. Given that the contact locus is distributed approximately uniformly along the two chain contours, this arm preferentially belongs to the shortest of the two chains. To optimize chain-length discrimination for probes experimentally, one should obviously choose hosts so that M is always greater than or equal to N.

The probe velocity during an entanglement is defined as the distance traveled by the probe divided by the

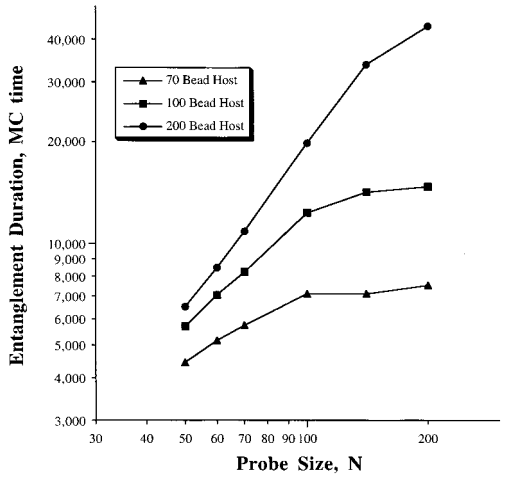

Figure 2. Average entanglement duration versus N for $M = 70$, 100, and 200.

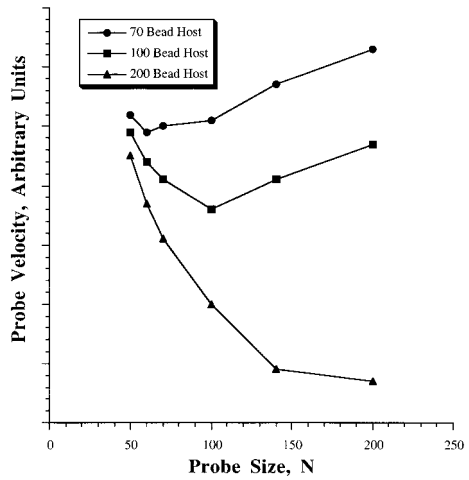

Figure 3. Probe velocity versus N for $M = 70$, 100, and 200. Minima occur at N approximately equal to M (although the lowest curve does not extend to sufficient N to confirm a minimum).

number of time steps between first contact and final release. Figure 3 plots the average probe velocity as a function of N for the three host sizes. The plot reveals a minimum of probe velocity at N approximately equal to M. This minimum and its location may explain an important experimental observation, that probes are best separated by a solution of comparably sized hosts. To understand the dynamics responsible for the minimum, one must consider two separate effects, the duration of an entanglement and the displacement of an entanglement. When probes are smaller than hosts, the first effect dominates, and a larger entanglement duration causes the probe velocity to decrease with increasing N. The entanglement displacement remains small, as only a small downfield probe force (proportional to N) counters a large host resistance. However, when probes are larger, the entanglement displacement strongly augments the overall probe motion, and the average probe velocity rises with N as a probe can now effectively drag a more mobile host downfield a considerable distance before release.

4. Conclusions

In a dilute host matrix, simulations reveal that the size and mobility of neutral hosts play an important role

in the electrophoretic size discrimination of polyelectrolyte probes. The key size-discriminating events are pairwise chain entanglement interactions that can be characterized in terms of three physically distinct parameters: the probability of entanglement (discussed extensively in a previous paper[16]), the average duration of entanglement, and the average displacement of entanglement. In a statistical sense, enntanglements most significantly hinder probe motion when probe and host sizes are nearly equal, and the strongest probe size discrimination occurs when probe sizes are less than or equal to the host size. Trends in capillary electrophoresis data appear consistent with the simulation picture, although the simulation itself does not frame a complete model for the experimentally measured bulk mobility, a parameter different than the molecular scale velocity presented here. To facilitate better comparisons of simulation with experiment, we have conducted experiments that systematically vary N and M for monodisperse probe and host. These studies will be reported separately. Within the context of electrophoresis in a dilute polymer matrix, the current simulations are the first to treat probe and host motions consistently. Whether a similarly consistent strategy can be developed for electrophoresis in a nondilute polymer matrix, an equally important problem, remains uncertain.

Acknowledgment. Financial support from the Materials Research Science and Engineering Center at the University of Massachusetts is gratefully acknowledged.

References and Notes

(1) Barron, A. E.; Soane, D. S.; Blanch, H. W. *J. Chromatogr.* **1993**, *652*, 3.
(2) Barron, A. E.; Blanch, H. W.; Soane, D. S. *Electrophoresis* **1994**, *15*, 597.
(3) Barron, A. E.; Sunada, E.; Blanch, H. W. *Electrophoresis* **1995**, *16*, 64.
(4) Minárik, M.; Gas, B.; Kenndler, E. *Electrophoresis* **1995**, *18*, 98.
(5) Poli, J. B.; Shure, M. R. *Anal. Chem.* **1992**, *64*, 896.
(6) Baba, Y.; Ishimaru, N.; Samata, K.; Tsuhaku, M. *J. Chromatogr.* **1993**, *653*, 329.
(7) Barron, A. E.; Sunada, W. M.; Blanch, H. W. *Biotechnol. Bioeng.* **1996**, *52*, 259.
(8) Chang, H. T.; Yeung, E. S. *J. Chromatogr.* **1995**, *669*, 113.
(9) Chiari, M.; Nesi, M. *J. Chromatogr.* **1993**, *652*, 31.
(10) Mitnik, L.; Salomé, L.; Viovy, J. L.; Heller, C. *J. Chromatogr.* **1995**, *710*, 309.
(11) Pulyaeva, H.; Garner, M. M.; Chrambach, A. *Electrophoresis* **1992**, *13*, 608.
(12) Cottet, H.; Gareil, P. *J. Chromatogr. A* **1997**, *772*, 369.
(13) Singhal, R. P.; Xian, J. *J. Chromatogr. A* **1993**, *652*, 47.
(14) Hubert, H. S.; Slater, G. W; Viovy, J. L. *Macromolecules* **1996**, *29*, 1006.
(15) Bünz, A. P.; Barron, A. E.; Prauznitz, J. M.; Blanch, H. W. *Ind. Eng. Res.* **1996**, *35*, 2900.
(16) Starkweather, M.; Muthukumar, M.; Hoagland, D. A. *Macromolecules* **1998**, *31*, 5495.
(17) Sevick, E. M.; Williams, D. R. M. *Phys. Rev. Lett.* **1996**, *76*, 2595.
(18) Saville, P. M.; Sevick, E. M. *Macromolecules* **1999**, *32*, 892.
(19) Metropolis, N.; Rosenbluth, A. W.; Rosenbluth, M. N.; Teller, A. H. *J. Chem. Phys.* **1953**, *21*, 1098.

MA990478R